# Particle size effects on the thermal behaviour of maghemite synthesised by flame pyrolysis

S. Grimm[a], T. Stelzner[b,*], J. Leuthäußer[a], S. Barth[a], K. Heide[b]

[a] *Friedrich-Schiller-Universität Jena, Institut für Anorganische und Analytische Chemie, A.-Bebel-Str. 6/8, 07743 Jena, Germany*
[b] *Friedrich-Schiller-Universität Jena, Institut für Geowissenschaften, Burgweg 11, 07749 Jena, Germany*

## Abstract

Thermal treatment of pure nanoscale maghemite ($\gamma$-$Fe_2O_3$) powders under argon yields different products depending on particle size. Particles with a mean diameter above 15 nm transform to hematite ($\alpha$-$Fe_2O_3$). Smaller particles, which were synthesised under identical conditions but from solutions with lower $Fe^{3+}$ concentrations, transform into magnetite ($Fe_3O_4$) during thermal treatment. This phenomenon can be explained by adsorbed or incorporated reducing carboxylate groups. The origin of the reducing species and possible reaction mechanisms with the maghemite particles are discussed. © 1997 Elsevier Science B.V.

## 1. Introduction

Preparation of $\gamma$-$Fe_2O_3$, with a different morphology and particle size, is of special interest for various applications (e.g. catalysts, magnetic pigments, and liquids), in view of particular chemical and physical properties of the products. One possible way of synthesis is the direct combustion of the flammable iron-containing solutions by means of an oxygen–hydrogen gas flame with a large excess of oxygen, which yields $\gamma$-$Fe_2O_3$ particles of a size directly dependent on the iron concentration of the preparation solution [1].

Maghemite is a metastable phase in the Fe–O system with a spinel structure. When heated in air, it is transformed to $\alpha$-$Fe_2O_3$ in the temperature range of 370–600°C [2]. The transformation temperature increases with decreasing particle size [3] and depends on the quantity and kind of impurities [4]. However, a phase transformation of $\gamma$-$Fe_2O_3$ to the related structure of $Fe_3O_4$ is also possible [5]. Therefore, a redox process involving reduction of one third of the $Fe^{3+}$ to $Fe^{2+}$ ions, and removal of oxygen from the lattice have to be taken into consideration. The reverse reaction, oxidation of $Fe_3O_4$ to $\gamma$-$Fe_2O_3$ at 250°C, is well known and technically used for the preparation of magnetic pigments [6].

In this paper we want to discuss possible reasons for the observed transformation of nanoscale $\gamma$-$Fe_2O_3$ particles to $Fe_3O_4$ during thermal treatment under low oxygen partial pressure.

---

*Corresponding author. Tel.: 00 49 3641 630241; fax: 00 49 3641 630281.

## 2. Experimental

### 2.1. Samples

The preparation of $\gamma$-$Fe_2O_3$ by flame pyrolysis and the properties of the powders thus obtained, are described in detail in [1] and summarised in Table 1. By means of X-ray diffraction, all powders were characterised as $\gamma$-$Fe_2O_3$. However, for powders with a very small particle size, the broadening of the peaks reflects an increasing degree of structural disorder or strain due to crystal defects and the presence of amorphous material. No indications for the existence of $Fe^{2+}$ could be obtained from Mössbauer spectroscopy [7]. The powders consist of dense spherical particles with a very low tendency to aggregate and agglomerate.

### 2.2. Thermal analysis

The thermal behaviour of the maghemite samples was measured under standard conditions with the following techniques:

- Simultaneous thermogravimetry (TG), derivative thermogravimetry (DTG), and heat-flux differential scanning calorimetry (heat-flux DSC – NETZSCH STA 429)
- Evolved gas analysis (EGA) by mass spectrometry (self-developed device in combination with Balzers QMG 420C [8]).

The experimental conditions can been seen from Table 2.

IR spectra were obtained with KBr pellets (1 mg sample per 200 mg KBr) on a PERKIN ELMER

Table 2
Experimental conditions

|  | TG–DTG–DSC | EGA |
| --- | --- | --- |
| Heating rate | 10 K/min | 10 K/min |
| Crucible material | Platinum | $Al_2O_3$ |
| Reference | Pt-crucible | — |
| Atmosphere | Argon (70 $cm^3$/min)/air | Vacuum $<10^{-3}$ Pa |
| Sample weight | 15–25 mg | 4–6 mg |

Model 2000 spectrometer. A PMI automated BET Sorptometer was used for sorption measurements and a LECO CS-225 analyser for determination of C-contents.

## 3. Results

### 3.1. DSC in air

All samples, except sample FPCO3 show two overlapping exothermic effects with peaks varying in a temperature range of ca. 150–300°C (Figs. 1–4, Table 3). The peak areas and intensities increase with decreasing particle size.

The phase transition of $\gamma$-$Fe_2O_3$ to $\alpha$-$Fe_2O_3$ occurs in a temperature range of ca. 450–600°C. The samples FPCO3, FPCO2 and FPCO1 show increasing exothermic effects with decreasing particle size. Sample FPACAC shows a double peak in this temperature region.

A weak endothermic peak at 675°C results from the magnetic phase transition of $\alpha$-$Fe_2O_3$ (from weak ferrimagnetism to paramagnetism) [9]. This effect is the only remaining during cooling down and rerunning the same sample through the same temperature range.

Table 1
Preparation solutions and product description of $\gamma$-$Fe_2O_3$ powders

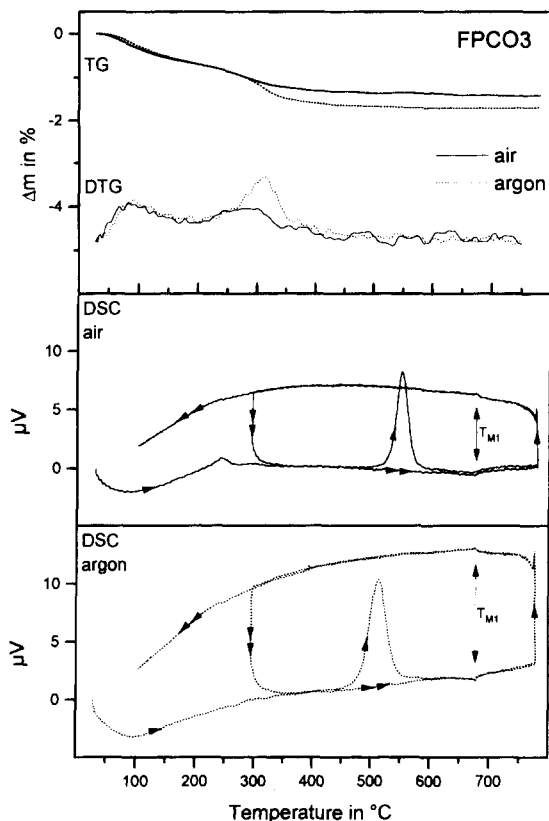|  | FPCO3 | FPCO2 | FPCO1 | FPACAC |
| --- | --- | --- | --- | --- |
| Iron compound for flame pyrolysis | $Fe(CO)_5$ | $Fe(CO)_5$ | $Fe(CO)_5$ | $Fe(acac)_3$ |
| $Fe^{3+}$ concentration in toluene (mol/l) | 3.6 | 1.8 | 0.5 | 0.3 |
| Identified product of flame pyrolysis | $\gamma$-$Fe_2O_3$ | $\gamma$-$Fe_2O_3$ | $\gamma$-$Fe_2O_3$ | $\gamma$-$Fe_2O_3$ |
| BET surface area ($m^2$/g) | 66 | 85 | 103 | 133 |
| Particle diameter by BET theory (nm) | 19 | 14 | 12 | 9 |
| Pore volume of the powder ($cm^3$/g) | 0.2 | 0.2 | 0.25 | 0.35 |
| Carbon content of the powder (wt%) | 0.2 | 0.6 | 2.0 | 1.7 |

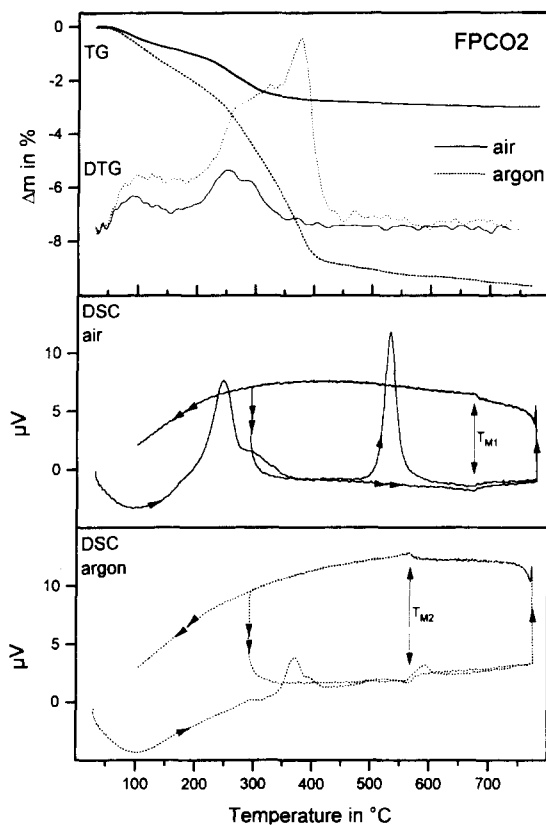Fig. 1. DSC, TG, and DTG curves of sample FPCO3 in air and under argon.



Fig. 2. DSC, TG, and DTG curves of sample FPCO2 in air and under argon.

Table 3
DSC and TG data of $\gamma$-Fe$_2$O$_3$ powders (peak temperature in °C)

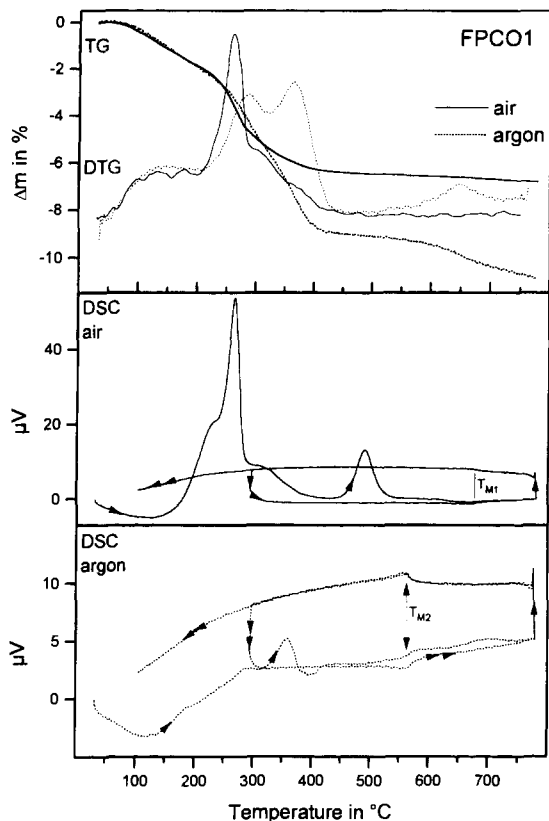| Sample, atmosphere | Exothermic reaction | | | Endothermic reactions | | Weight loss in % (25–780°C) |
|---|---|---|---|---|---|---|
| | Oxidation | Crystallisation | Inversion | Neelpoint | | |
| | | | | $T_{M1}$ | $T_{M2}$ | |
| FPCO3 | | | | | | |
| Air | — | 244 | 552 | 675 | | 1.4 |
| Argon | — | — | 512 | 675 | | 1.7 |
| FPCO2 | | | | | | |
| Air | (176) | 248 | 533 | 674 | | 3.0 |
| Argon | — | 370 | — | — | 567 | 9.6 |
| FPCO1 | | | | | | |
| Air | 226 | 265 | 489 | 673 | | 6.8 |
| Argon | — | 357 | — | — | 562 | 10.9 |
| FPACAC | | | | | | |
| Air | 215 | 263 | 543, 585 | 675 | | 5.5 |
| Argon | — | 374 | — | — | 565 | 8.6 |

Fig. 3. DSC, TG, and DTG curves of sample FPCO1 in air and under argon.
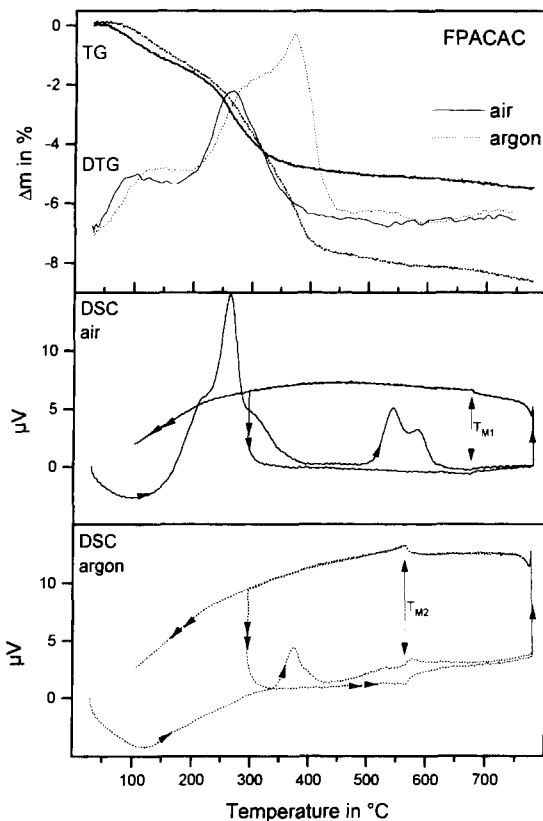


Fig. 4. DSC, TG, and DTG curves of sample FPACAC in air and under argon.

## 3.2. DSC under argon

DSC curves of samples FPCO2, FPCO1 and FPA-CAC under argon (ca. 10 ppm $O_2$) show a single exothermic peak around 370°C (Figs. 2–4). The transition of $\gamma$-$Fe_2O_3$ to $\alpha$-$Fe_2O_3$ (512°C) can be seen only for the sample with the biggest particle size, FPCO3 (Fig. 1). Hence, this sample alone shows the Neel-point of $\alpha$-$Fe_2O_3$ (675°C). In contrast, all other samples show the magnetic phase transition of $Fe_3O_4$ (ca. 565°C, [6]) during heating and cooling.

After heat treatment under argon, all powders, except for the sample FPCO3 show a black colour, are strongly magnetic, and can be identified by X-ray diffraction as $Fe_3O_4$. The presence of the typical $Fe^{2+}$ VIS/NIR peak in the remission spectra as well as cerimetric redox titration proved the existence of $Fe^{2+}$. Hence, a formation of elemental carbon as a

source for the black colour of the powders can be excluded.

## 3.3. TG in air and under argon

The TG curves prove the results of the DSC measurements (Figs. 1–4). The sample FPCO3 shows only a weak weight loss up to 350°C, which is obviously due to the desorption of a monolayer of physically adsorbed gases (e.g. 1 $m^2$ of a monolayer of adsorbed $H_2O$ corresponds to 0.278 mg).

The TG curves of the samples with the smaller particle sizes yield the following results:

- The weight losses under argon are considerably higher and continue at higher temperatures.
- After crystallisation (ca. 300°C in air and ca. 400°C under argon), no further significant weight loss is observed.

• The weight losses under argon are always more than 3.34% higher compared with the weight losses in air. That implies, besides desorption of physically and chemically adsorbed gases, the release of oxygen can occur according the following formal equation:

$$Fe_2O_3 \rightarrow \tfrac{2}{3}Fe_3O_4 + \tfrac{1}{6}O_2 \quad (\Delta m = 3.34\%)$$
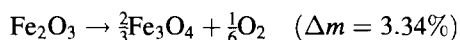
## 3.4. Evolved gas analysis

Fig. 5 shows the release of principal volatiles from the investigated powders. The measurements yield ion currents, which are proportional to the partial pressures of the various volatiles released from the sample as a function of temperature. The
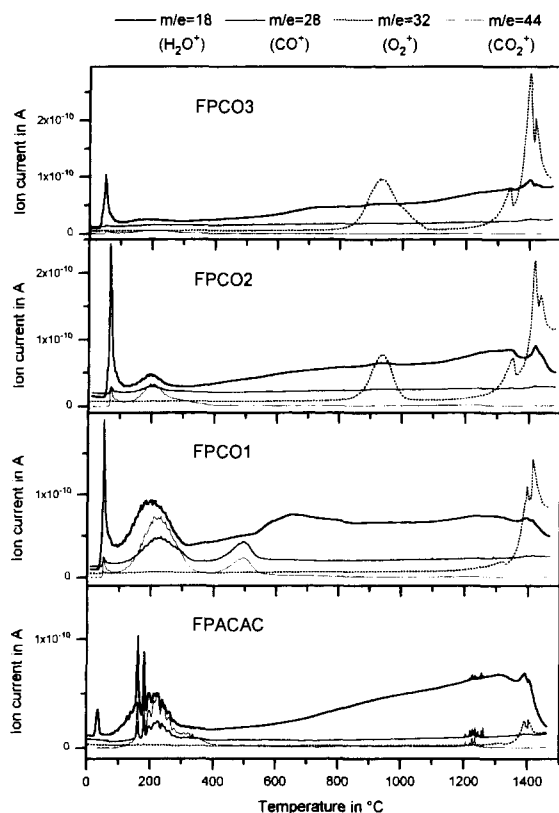


Fig. 5. Evolved gas analysis curves on heating γ-Fe₂O₃ powders under vacuum conditions, showing release of principal volatiles from 25–1500°C.

fragmentation effects, isotopic abundances, and background contributions have to be considered for an interpretation of the evolved gas analysis curves. As for example, the parent mass peak $m/e=44$ was measured for the volatile $CO_2$. In cases, where more than one species can share the same $m/e$ values (e.g. $N_2^+$ and $CO^+$ at $m/e=28$), the fragment peaks were used to distinguish among possible volatiles.

With decreasing particle size, increasing amounts $H_2O$ ($m/e=18$) are released below 300°C. Furthermore, a second peak appears at ca. 200°C besides the peak below 100°C. For the sample with the smallest particle size (FPACAC), the amount of evolved $H_2O$ decreases slightly, and the peak at ca. 200°C shows a multistage nature. The $H_2O$ release is probably due to the decomposition of amorphous Fe-oxohydroxides, which have been investigated for their dependence on crystallinity in Ref. [10]. Physically and chemically adsorbed $H_2O$ is lost at room temperature in vacuum prior to analysis, or driven off over a wide temperature range.

In accordance with the increasing water release, the peak intensities of $CO_2$ ($m/e=44$) and CO ($m/e=28$) increase in the temperature range of ca. 50–350°C. The well-defined peaks indicate an incorporation of carbon containing species into the crystal structure of the Fe-oxohydroxides. Fe-carbonate could be responsible for the CO and $CO_2$ peaks shown by sample FPCO1 at ca. 500°C, and the host phase of the released CO and $CO_2$ from sample FPACAC at ca. 1220°C still remains unclear.

The sample FPCO3 shows the typical oxygen peaks due to the reduction of $Fe_2O_3$ to $Fe_3O_4$ (800–1000°C) and $Fe_3O_4$ to FeO (>1200°C) under vacuum conditions [10]. The second oxygen peak is structured due to phase equilibria in the $Fe_2O_3$-FeO system [11]. The amount of released oxygen, in both regions, decreases with decreasing particle size. Finally, the oxygen peak of the hematite-magnetite transformation completely disappears (samples FPCO1 and FPACAC).

Some fragments of organic compounds are liberated predominantly from the powders with the smallest particles. However, the corresponding ion currents are, by two orders of magnitude, lower than those of the dominating gas specimen.

Table 4
Typical absorbance peaks of carbonate and carboxylate complexes in an IR spectrum

| Compound | Wave number/ $(cm^{-1})$ | | | | | |
|---|---|---|---|---|---|---|
| Monodentate carbonate complex | 1453 | 1373 | 1070 | 850 | 756 | 678 |
| Bidentate carbonate complex | 1593 | 1265 | 1030 | 834 | 760 | 673 |
| Covalent bonded bidentate carbonate group | 1870 | 1260 | | | | |
| Ionic carbonate group | 1460 | | 1096 | | 735 | |
| Ionic carboxylate group | 1550–1610 | 1410 | | | | |

## 3.5. IR spectroscopy

According to HAIR [12], the absorbance peaks from some typical carbonate- and carboxylate-complexes in an IR spectrum (Table 4) can also be assigned to these specimens adsorbed onto oxide surfaces. However, the following problems have to be considered:

- Shift of peaks due to changes of symmetry in the adsorbed state, appearance of new peaks;
- Existence of different adsorption places at one oxide surface;
- Differences in acidity or basicity between various oxides;
- Influence of various crystalline modifications; and
- Different oxidation states of the cations and charge transfers.

IR spectra of the $\gamma$-Fe$_2$O$_3$ powders (Fig. 6) show the presence of OH, CO$_3^{2-}$, and COO$^-$. With decreasing particle size increases the intensity of the peaks in the 1300 to 1700 cm$^{-1}$ range. Together with the rather weak peak at 1000 cm$^{-1}$, this gives evidence for the predominance of carboxylate compared with carbonate. CO can be excluded because of the absence of a peak at ca. 2000 cm$^{-1}$. Furthermore, adsorbed H$_2$O (3000–3500 cm$^{-1}$) and CO$_2$ (double peak at ca. 2300 cm$^{-1}$) can be seen against the background of air.



Fig. 6. IR spectra of $\gamma$-Fe$_2$O$_3$ powders showing the absorbance peaks of the carboxylate ion.

## 4. Discussion

The samples with the smaller particle size (FPCO2, FPCO1, FPACAC) show two exothermic effects in a temperature range of ca. 150–300°C, which are due to an oxidation of surface adsorbates in air and the crystallisation of amorphous constituents, respectively. Unde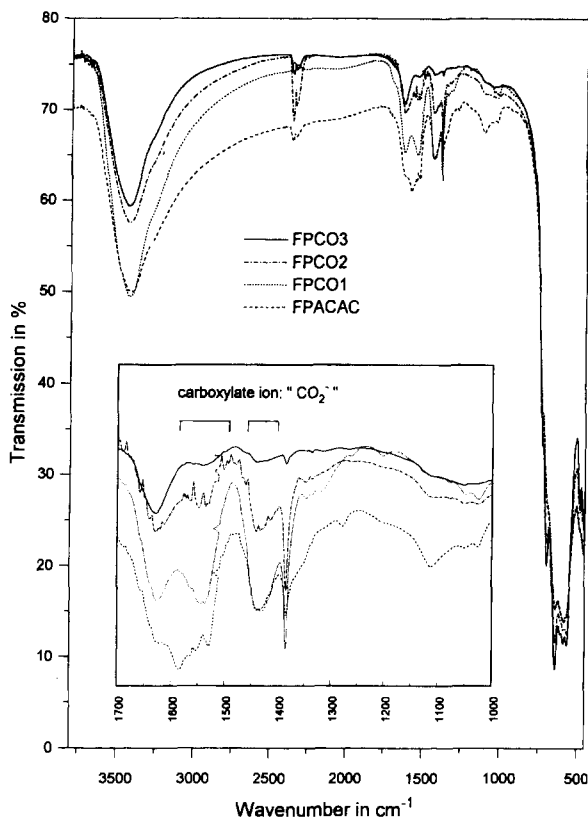r argon, the oxidation of adsorbates is prevented. Consequently, the reducing species adsorbed onto the small $\gamma$-Fe$_2$O$_3$ particles during thermal treatment affect a phase transformation to Fe$_3$O$_4$. Upon heating bigger particles (FPCO3), the above-mentioned 'low-temperature reduction' does not yield Fe$_3$O$_4$; instead $\alpha$-Fe$_2$O$_3$ is formed.

The carbon content of the powders increases by a factor of 10 with decreasing particle size (Table 1); this means that there is no linear correlation between
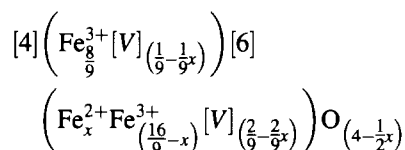
the surface area or the pore volume and the C-content. From sorption measurements also no indications for an increased amount of micropores in the small particles can be derived [1]. Therefore, multilayers or more complex adsorbates should exist. The increasing peak intensities of the carboxylate ion in the IR spectra could be due to increasing adsorption onto the smaller particles. The calculation of the number of adsorbed layers on the basis of the estimated C-contents in case of pure $COO^-$ gives the following results: FPCO3 = 0.3, FPCO2 = 0.6, FPCO1 = 2 FPACAC = 1.2. The reasons for increased adsorption could be a more activated state of the smaller particles (energy gain by growth) or a higher amount of defects at the surface. A second possibility is the structural incorporation of water and carboxylate into the highly disordered $\gamma$-$Fe_2O_3$ structure. The stabilising effect of water incorporation on the $\gamma$-phase is well known [13]. The formation and incorporation of carboxylate could occur during particle synthesis in the gas flame. Despite the larger oxygen excess in the flame, iron can exist in the divalent state on account of the high temperature. In contrast to the $Fe^{3+}$ ion, the increased radius of the $Fe^{2+}$ ion enables the quick adsorption of $CO_2$, which is available from the combustion of the solvent.

Furthermore, the $Fe^{2+}$ ion prefers a high coordination number [6]. $CO_2$ can act as a bidentate ligand in the following manner (surface carboxylate with electron transfer), see Fig. 7.

The constitution of the adsorbate complex is stabilised because of the easy release of an electron from $Fe^{2+}$, as also due to the structural change of the linear $CO_2$ molecule to a bidentate ligand by gaining an electron. Furthermore, the carboxylate formation is preferred because of kinetic reasons in comparison to the oxidation of the $Fe^{2+}$ with molecular oxygen. The very short retention time of the particles in the flame apparently favours the one-electron transfer from $Fe^{2+}$ to $CO_2$. However, molecular oxygen has to give off

two electrons and, in addition, the oxygen ion has to be incorporated into the lattice of the iron oxide in a complex manner [5].

Calculating the theoretical amount of carboxylate ions necessary for stoichiometric yield of $Fe_3O_4$ from $\gamma$-$Fe_2O_3$ (15.5 wt%) reveals that, probably, the $Fe^{2+}$ formed earlier, prevents the formation of $\alpha$-$Fe_2O_3$. As a result, the transformation to $Fe_3O_4$ is continued by the following solid solution:

$$[4]\left( Fe^{3+}_{\frac{8}{9}}[V]_{\left(\frac{1}{9}-\frac{1}{9}x\right)} \right)[6]$$
$$\left( Fe^{2+}_x Fe^{3+}_{\left(\frac{16}{9}-x\right)}[V]_{\left(\frac{2}{9}-\frac{2}{9}x\right)} \right)O_{\left(4-\frac{1}{2}x\right)}$$

where: $(0 \leq x \leq 1)$, and $V$ – vacancy

Cerimetric titration determinations for the sample FPACAC showed, that up to 450°C, about two-thirds, and up to 600°C, about three-quarters of the $Fe^{2+}$ is formed in $Fe_3O_4$. Therefore, it can be understood, that the oxygen peak at ca. 900°C, detected in the EGA curves for powders with bigger particles, disappears with decreasing particle size.

Morando et al. [14] reported, that during the thermal decomposition of $Fe(HCOO)_3 \cdot 2H_2O$ in nitrogen, $\alpha$-$Fe_2O_3$ is also formed besides $Fe_3O_4$ even in the presence of reducing species, particularly the formiat anion. In contrast to this, our experiments show that even in case of nanosized $\gamma$-$Fe_2O_3$ particles (5–20 nm), less than stoichiometric amounts of reducing species are sufficient to prevent the transition to $\alpha$-$Fe_2O_3$. This points out the strong influence of morphological properties, besides redox conditions, on the thermal behaviour of iron oxides. Probably, the very short diffusion paths make it easier to remove the oxygen before the nuclei of $\alpha$-$Fe_2O_3$ are formed and reach the critical size for growth. The phase transition of $\gamma$-$Fe_2O_3$ to $Fe_3O_4$ is then accompanied with a crystal growth on account of the high sinter ability of the nanosized powders.
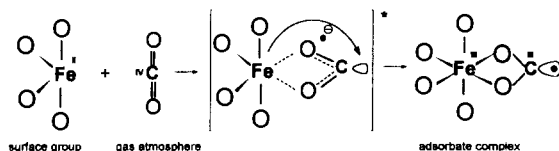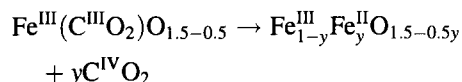
## 5. Conclusions

Maghemite was synthesised from iron-containing solutions by flame pyrolysis. With decreasing concentration of Fe in the preparation solution, the particle size of the product decreases. At the same time



Fig. 7.

the chemical composition of the powders increasingly changes due to adsorption or incorporation of $H_2O$, $CO_3^{2-}$, and $COO^-$. Considering the strong oxidizing conditions during formation of the particles in the gas flame, it is surprising that reducing species like $COO^-$ can be found in the resulting powders. In contrast to similar gas phase reactions [14], no $Fe^{2+}$ is present in the product.

Kinetic effects are, probably, mainly responsible for the formation of the reducing species during particle synthesis. On account of the high temperature in the flame, $Fe^{2+}$ is intermediately formed. From this $Fe^{2+}$, an electron transfer can take place to the adsorbed $CO_2$. Apparently, the very short retention time favours this one-electron reaction with $CO_2$ in contrast to the two-electron reaction with $O_2$. Amounts of carboxylate species, even less than stoichiometric, adsorbed onto the $\gamma$-$Fe_2O_3$, prevent the transformation to $\alpha$-$Fe_2O_3$ during heating the powders in an inert atmosphere. Instead, $Fe_3O_4$ is formed according to the following equation:

$$Fe^{III}(C^{III}O_2)O_{1.5-0.5} \rightarrow Fe^{III}_{1-y}Fe^{II}_yO_{1.5-0.5y}$$
$$+ yC^{IV}O_2$$

## Acknowledgements

## References

[1] St. Grimm, M. Schultz, R. Müller and St. Barth, J. Mater. Sci., in press.

[2] R.C. Mackenzie, The Differential Thermal Investigation of Clays, Mineralogical Society, London (1957).

[3] B. Gillot, H. Novaim, F. Mathieu and A. Rousset, Mater. Chem. Phys., 27 (1991) 287.

[4] E. Wolska and U. Schwertmann, Solid State Ionics, 32/33 (1989) 214.

[5] A.F. Wells, Structural Inorganic Chemistry, Clardon Press, Oxford (1975) 456.

[6] U. Schwertmann and R.M. Cornell, Iron Oxides in the Laboratory, VCH Verlagsgesellschaft, Weinheim, New York, Basel, Cambridge (1991) 11.

[7] K. Schäfer, Universität Leipzig, personal communication.

[8] E. Hartmann, Th. Stelzner and K. Heide, Glastech. Ber. Glass Sci. Technol., 68 (1995) 107.

[9] D. Schultze, Differentialthermoanalyse, Deutscher Verlag der Wissenschaften, Berlin (1969) 228.

[10] Th. Stelzner and K. Heide, Meteoritics & Planetary Science, 31 (1996) 249.

[11] L.S. Darken and R.W. Gurry, J. Am. Chem. Soc., 68 (1946) 799.

[12] M.L. Hair, Infrared spectroscopy in surface chemistry, Marcel Dekker Inc., New York (1967).

[13] P.B. Braun, Nature, 170 (1952) 1123.

[14] P.J. Morando, N.H. Piacquadio, M.A. Blesa and C.O.D. Vedova, Thermochim. Acta, 117 (1987) 325.